European Congress on Computational Methods in Applied Sciences and Engineering
ECCOMAS Computational Fluid Dynamics Conference 2001
Swansea, Wales, UK, 4-7 September 2001

HIGH ORDER DIFFERENCE METHOD FOR LOW MACH NUMBER AEROACOUSTICS

Bernhard Müller

Department of Scientific Computing, Information Technology, Uppsala University,
S-751 04 Uppsala, Sweden, e-mail: bernd@tdb.uu.se,
web page: http://www.tdb.uu.se/∼bernd/

Key words: Euler equations, entropy splitting, low Mach number aeroacoustics, high order difference method, summation by parts.

Abstract. *The Euler equations are split into a conservative and a symmetric non-conservative portion to allow the derivation of a generalized energy estimate. Owing to the large disparity of acoustic and stagnation quantities in low Mach number aeroacoustics, the split Euler equations are formulated in perturbation form. While the conventional central sixth-order accurate stencil is employed in the interior, the difference method is third-order accurate at the boundary to satisfy the summation by parts property analogous to the integration by parts in the continuous energy estimate. Since thereby a discrete energy estimate is automatically satisfied, strict stability of the high order difference method is guaranteed. The boundary conditions are implemented by a penalty term. The classical Runge-Kutta method is used for time integration. Spurious oscillations are suppressed by a new characteristic-based filter. The method has been applied to simulate vortex sound at low Mach numbers. The computed acoustic pressure generated by an almost circular Kirchhoff vortex is in excellent agreement with the analytical solution.*

1 INTRODUCTION

High order numerical methods are preferred in the emerging area of computational aeroacoustics (CAA) to satisfy the stringent accuracy requirements [25][27]. Since high order methods can accurately represent a wave with a few grid points, they are more efficient than low order methods, e.g. second-order methods., in terms of computing time and memory [6].

Recently, high order finite difference methods have been developed, which are constructed to be strictly stable for linear hyperbolic and parabolic problems [7][23]. These methods satisfy the summation by parts (SBP) property, which is analogous to integration by parts in the continuous energy estimate. They have been applied to linear equations [24] and the nonlinear Euler and Navier-Stokes equations [4][5][16]. If a nonlinear conservation law can be canonicly split into a conservative portion and a symmetric non-conservative portion, a continuous energy estimate can be derived and strict stability can be proved for SBP operators [20][19].

Since the symmetrization of the nonlinear Euler equations is based on entropy related variables, the canonical splitting of the flux derivatives for the nonlinear Euler equations was termed "entropy splitting" by Yee et al. [28][30][26]. They showed that the split form of the the Euler equations requires less numerical dissipation than its un-split counterpart in association with non-dissipative spatial central schemes [30][29].

Owing to the large disparity of acoustic and stagnation quantities in low Mach number aeroacoustics, we reformulate the split Euler equations in terms of perturbation variables. For the conservative portion, the changes of the conservative variables with respect to their stagnation values are used [22][15][21]. The entropy variables in the non-conservative portion are expressed similarly. Nonlinearities and the conservative portion of the split flux derivatives are retained. The perturbation form (without entropy splitting) was shown to minimize numerical cancellation errors compared to the original conservation laws [22] and has been successfully applied to low Mach number CAA [15][21].

For the discretization, a sixth-order central interior scheme with a third-order boundary scheme that satisfies a discrete analogue of the integration by parts procedure used in the continuous energy estimate (summation by parts (SBP) property) is employed [23]. If the physical boundary conditions (BCs) are implemented correctly and if the split form of the inviscid flux derivatives is used, **nonlinear stability** of the nonlinear Euler equations [4][5][19] is obtained. Characteristic and nonreflecting BCs, if needed, are imposed at each time step either by injection or by a simultaneous approximation term (SAT) [1]. To suppress the spurious high frequency oscillations associated with central schemes, modified versions of the characteristic-based filter method of Yee et al. [28] are used. The metric terms in the general coordinate transformation are discretized by the same difference operator as the flow variables leading to freestream preservation (uniform flow conservation) [26] for the conservative portion of the split equations. The time derivative is approximated by the classical fourth-order explicit Runge-Kutta method with careful

treatment of the intermediate BC at the different stages of the Runge-Kutta method to minimize the loss of global accuracy of the scheme [2][6][9].

The numerical method has been applied to the computation of vortex sound. The prediction of vortex sound has been one of the most important goals in computational aeroacoustics (CAA), because the noise in turbulent flow is generated by vortices. Here, we focus on the numerical simulation of a single vortex, namely the Kirchhoff vortex, to verify the high order finite difference method for the 2D Euler equations. The Kirchhoff vortex is an elliptical patch of constant vorticity rotating with constant angular frequency in irrotational flow. The acoustic pressure generated by the Kirchhoff vortex is governed by the 2D Helmholtz equation, which can be solved analytically for almost circular Kirchhoff vortices using separation of variables [14]. The sound emitted by rotor induced deformations of an electric generator casing is governed by the same 2D Helmholtz equation and can be solved in the same way as for the Kirchhoff vortex sound [21]. In [15][21], the present high order difference method was applied to simulate Kirchhoff vortex sound and generator sound using injection instead of SAT to impose boundary conditions and another form of the characteristic-based filter.

The outline of the paper is as follows. The entropy splitting perturbation form of the Euler equations is derived in Section 2. The high order difference method satisfying the SBP property is outlined in Section 3. The analytical solution and numerical results with the high order difference method for the sound generated by an almost circular Kirchhoff vortex are discussed in Section 4.

2 FORMULATION OF THE EULER EQUATIONS

2.1 Canonical Splitting

The canonical splitting is reviewed for a 1D nonlinear conservation law [20][19][4][5][26]

$$\mathbf{U}_t + \mathbf{F}(\mathbf{U})_x \;=\; 0\,, \tag{1}$$

where $\mathbf{U}$ denotes the vector of the conservative variables and $\mathbf{F}$ the nonlinear flux vector. We assume that so-called entropy variables $\mathbf{W} = \mathbf{W}(\mathbf{U})$ exist such that equation (1) can be transformed to

$$\mathbf{U}_\mathbf{W}\mathbf{W}_t + \tilde{\mathbf{F}}_\mathbf{W}\mathbf{W}_x \;=\; 0\,, \tag{2}$$

where the Jacobian matrix $\mathbf{U}_\mathbf{W}$ is symmetric and positive definite and the Jacobian matrix $\tilde{\mathbf{F}}_\mathbf{W}$ is symmetric. We use the notation $\tilde{\mathbf{F}}(\mathbf{W}) = \mathbf{F}(\mathbf{U}(\mathbf{W}))$. Moreover, we require the functions $\mathbf{U}(\mathbf{W})$ and $\tilde{\mathbf{F}}(\mathbf{W})$ to be homogeneous of degree $\beta \neq -1$, i.e. there is a constant $\beta \neq -1$ such that for all $\sigma \in \mathbb{R}$

$$\mathbf{U}(\sigma\mathbf{W}) = \sigma^\beta \mathbf{U}(\mathbf{W}), \tag{3}$$
$$\tilde{\mathbf{F}}(\sigma\mathbf{W}) = \sigma^\beta \tilde{\mathbf{F}}(\mathbf{W}). \tag{4}$$

They satisfy Euler's ordinary differential equations

$$\mathbf{U}_\mathbf{W}\mathbf{W} = \beta\mathbf{U}, \tag{5}$$
$$\tilde{\mathbf{F}}_\mathbf{W}\mathbf{W} = \beta\tilde{\mathbf{F}}. \tag{6}$$

We introduce the canonical splitting

$$\mathbf{U}_t = \frac{\beta}{\beta+1}\mathbf{U}(\mathbf{W})_t + \frac{1}{\beta+1}\mathbf{U}_\mathbf{W}\mathbf{W}_t, \tag{7}$$
$$\tilde{\mathbf{F}}_x = \frac{\beta}{\beta+1}\tilde{\mathbf{F}}(\mathbf{W})_x + \frac{1}{\beta+1}\tilde{\mathbf{F}}_\mathbf{W}\mathbf{W}_x. \tag{8}$$

If we consider the conservation law (1) in the interval $[0,1]$ and use the postive definiteness of $\mathbf{U}_\mathbf{W}$, the energy norm is defined by

$$||\mathbf{W}||_U^2 = (\mathbf{W}, \mathbf{U}_\mathbf{W}\mathbf{W}) = \int_0^1 \mathbf{W}^T\mathbf{U}_\mathbf{W}\mathbf{W}\,dx. \tag{9}$$

Then, the canonical splitting, symmetry of the Jacobian matrices, Euler's ODEs and integration by parts allow to derive the equation

$$\frac{d}{dt}||\mathbf{W}||_U^2 = \frac{d}{dt}(\mathbf{W}, \mathbf{U}_\mathbf{W}\mathbf{W}) = -\mathbf{W}^T\tilde{\mathbf{F}}_\mathbf{W}\mathbf{W}|_0^1. \tag{10}$$

With the characteristic variables $\boldsymbol{\psi} = \tilde{\mathbf{R}}^T\mathbf{W}$, where $\tilde{\mathbf{F}}_\mathbf{W} = \tilde{\mathbf{R}}\tilde{\mathbf{\Lambda}}\tilde{\mathbf{R}}^T$, the following generalized energy estimate can be derived [20]

$$\frac{d}{dt}||\mathbf{W}||_U^2 \leq -\boldsymbol{\psi}^T\tilde{\mathbf{\Lambda}}^-\boldsymbol{\psi}|_{x=1} + \boldsymbol{\psi}^T\tilde{\mathbf{\Lambda}}^+\boldsymbol{\psi}|_{x=0}. \tag{11}$$

where $\tilde{\mathbf{\Lambda}}^\pm = \frac{1}{2}(\tilde{\mathbf{\Lambda}} \pm |\tilde{\mathbf{\Lambda}}|)$. Thus, if the ingoing characteristic variables, i.e. those components ψ_l at $x=1$ for which $-\tilde{\lambda}_l^-|_{x=1} > 0$ and those components ψ_l at $x=0$ for which $\tilde{\lambda}_l^+|_{x=0} > 0$ are prescribed as boundary conditions, the energy at any time t can be estimated in terms of the initial and boundary conditions. Consequently, the problem is well-posed. For homogeneous boundary conditions, the energy does not increase.

2.2 Entropy Splitting

In Cartesian coordinates, the 2D Euler equations can be expressed as

$$\mathbf{U}_t \; + \; \mathbf{F}_{1x} \; + \mathbf{F}_{2y} \; = \; 0 \, , \tag{12}$$

where

$$\mathbf{U} = \begin{pmatrix} \rho \\ \rho u \\ \rho v \\ \rho E \end{pmatrix} , \; \mathbf{F}_1 = \begin{pmatrix} \rho u \\ \rho u u + p \\ \rho v u \\ (\rho E + p) u \end{pmatrix} , \; \mathbf{F}_2 = \begin{pmatrix} \rho v \\ \rho u v \\ \rho v v + p \\ (\rho E + p) v \end{pmatrix} .$$

ρ denotes the density, u and v the x- and y-direction velocities, E the specific total energy, and p the pressure. The density ρ, pressure p, temperature T and specific internal energy e are related by the equations of state for a perfect gas $p = \rho R T$ and $e = c_v T$, where $R = c_p - c_v$ is the specific gas constant, and c_p and c_v are the specific heats at constant pressure and volume, respectively. We shall use $\gamma = \frac{c_p}{c_v} = 1.4$ for air. Using the equations of state and the definition of $E = e + \frac{1}{2}|\mathbf{u}|^2$, the pressure can be expressed as $p \; = \; (\gamma - 1)(\rho E - \frac{1}{2}\rho |\mathbf{u}|^2 \, ,$ where $\mathbf{u} = (u, v)^T$ denotes the velocity vector.

Harten [8] derived suitable entropy variables $\mathbf{W}$ for the Euler equations of perfect gas by defining

$$\mathbf{W}^T = \eta_{\mathbf{U}} \, , \tag{13}$$

i.e. the Jacobian matrix of the scalar and convex function $\eta = \rho h(S)$, where $S = ln(p/\rho^\gamma)$ is the nondimensional physical entropy and $h(S) = \beta exp(S/((1-\gamma)\beta))$. With this choice of $\mathbf{W}$, the homogeneity properties (3) (4), the symmetry of the Jacobian matrices and the positive definiteness of $\mathbf{U}_{\mathbf{W}}$ are satisfied. The entropy variables can be expressed as

$$\mathbf{W} = \frac{p^*}{p} \left[\rho E + \tilde{\alpha} p, -\rho u, -\rho v, \rho \right]^T \, , \tag{14}$$

where $p^* = -(p/\rho^\gamma)^{\frac{1}{\beta(1-\gamma)}}$ and $\tilde{\alpha} = -(\beta + 1 + \frac{2}{\gamma - 1})$. Yee et al. [30] discuss the choice of the parameter β: it must be chosen to fulfill either $\beta < \frac{\gamma}{1-\gamma}$ or $0 < \beta$.

For the discretization of the Euler equations, we shall only need to use the split flux derivatives. Thus, we consider the following split form of the Euler equations

$$\mathbf{U}_t \; + \; \frac{\beta}{\beta + 1} (\mathbf{F}_{1x} + \mathbf{F}_{2y}) \; + \; \frac{1}{\beta + 1} (\tilde{\mathbf{F}}_{1\mathbf{W}} \mathbf{W}_x + \tilde{\mathbf{F}}_{2\mathbf{W}} \mathbf{W}_y) \; = \; 0 \, , \tag{15}$$

where $\tilde{\mathbf{F}}_l = \mathbf{F}_l(\mathbf{U}(\mathbf{W}))$. The Jacobian matrices $\tilde{\mathbf{F}}_{l\mathbf{W}}, l = 1, 2$, cf. [4][28][30] and the entropy variables $\mathbf{W}$ can be expressed as functions of the conservative variables $\mathbf{U}$, cf. (14). The extension of entropy splitting to only thermally perfect gas and to time dependent curvilinear coordinates is outlined in [26].

2.3 Perturbation Form

In low Mach number aeroacoustics, the changes in the thermodynamic quantities are much smaller than their reference values. For example, the acoustic pressure p' is usually many orders of magnitude lower than the stagnation pressure p_0. Computing small differences of large numbers on the computer leads to cancellation. The formulation introduced in [22] is used to minimize numerical cancellation error for compressible low Mach number flow. The split Euler equations (15) are expressed in terms of the changes of the conservative variables with respect to their stagnation values. In Cartesian coordinates, the perturbed split 2D Euler equations can be written as

$$\mathbf{U'}_t + \frac{\beta}{\beta+1}(\mathbf{F'}_{1x} + \mathbf{F'}_{2y}) + \frac{1}{\beta+1}(\tilde{\mathbf{F}}_{1\mathbf{W}}\mathbf{W}_x + \tilde{\mathbf{F}}_{2\mathbf{W}}\mathbf{W}_y) = 0\,, \tag{16}$$

where

$$\mathbf{U'} = \begin{pmatrix} \rho' \\ (\rho u)' \\ (\rho v)' \\ (\rho E)' \end{pmatrix},\ \mathbf{F'}_1 = \begin{pmatrix} (\rho u)' \\ (\rho u)'u' + p' \\ (\rho v)'u' \\ (\rho H)'u' + (\rho H)_0 u' \end{pmatrix},$$

$$\mathbf{F'}_2 = \begin{pmatrix} (\rho v)' \\ (\rho u)'v' \\ (\rho v)'v' + p' \\ (\rho H)'v' + (\rho H)_0 v' \end{pmatrix}.$$

with

$$\rho' = \rho - \rho_0, \qquad (\rho\mathbf{u})' = \rho\mathbf{u}, \qquad (\rho E)' = \rho E - (\rho E)_0\,,$$

$$\mathbf{u}' = \frac{(\rho\mathbf{u})'}{\rho_0 + \rho'}, \qquad p' = (\gamma - 1)[(\rho E)' - \frac{1}{2}(\rho\mathbf{u})' \cdot \mathbf{u}'], \qquad (\rho H)' = (\rho E)' + p'.$$

In the Jacobian matrices $\tilde{\mathbf{F}}_{l\mathbf{W}}, l = 1, 2$, and in the entropy variables $\mathbf{W}$, $\rho, \rho E$ and p are replaced by $\rho_0 + \rho'$, $(\rho E)_0 + (\rho E)'$ and $p_0 + p'$, respectively. ρu and ρv coincide with the corresponding perturbation variables. For low Mach number CAA, we use the simplification that the flow is isentropic to set $p^* = -1$.

$w_{4x} = \left(\frac{p^*}{p}(\rho + \rho')\right)_x$ is evaluated from

$$w_{4x} = \left(\frac{p^*\rho_0}{p}\right)_x + \left(\frac{p^*}{p}\rho'\right)_x$$

to minimize the cancellation error with discretization. The first derivative on the right hand side is approximated by

$$\left(\frac{p^*\rho_0}{p}\right)_x \approx -\frac{p^*\rho_0}{p_0^2}\,p'_x\,,$$

i.e. we approximate p^2 by p_0^2 in the denominator of the right hand side. The approximation simplifies the implementation and could easily be replaced by the exact expression. w_{1x} is treated similarly and likewise the corresponding y-derivatives.

General geometries are treated by a coordinate transformation $x(\xi,\eta)$ $y(\xi,\eta)$. Thus, the perturbed split 2D Euler equations (16) are transformed to

$$\hat{\mathbf{U}}'_t \;+\; \frac{\beta}{\beta+1}(\hat{\mathbf{F}}'_{1\xi}+\hat{\mathbf{F}}'_{2\eta}) \;+\; \frac{1}{\beta+1}J^{-1}(\nabla\xi\cdot\tilde{\mathbf{F}}_{\mathbf{W}}\mathbf{W}_\xi+\nabla\eta\cdot\tilde{\mathbf{F}}_{\mathbf{W}}\mathbf{W}_\eta) \;=\; 0\,, \tag{17}$$

where

$$\hat{\mathbf{U}}' = J^{-1}\mathbf{U}'\,, \qquad \hat{\mathbf{F}}'_1 = J^{-1}\xi_x\mathbf{F}'_1 \;+\; J^{-1}\xi_y\mathbf{F}'_2\,, \qquad \hat{\mathbf{F}}'_2 = J^{-1}\eta_x\mathbf{F}'_1 \;+\; J^{-1}\eta_y\mathbf{F}'_2\,,$$

with the Jacobian determinant of the transformation $J^{-1} = \frac{\partial x}{\partial\xi}\frac{\partial y}{\partial\eta} - \frac{\partial x}{\partial\eta}\frac{\partial y}{\partial\xi}$, and the metric terms $J^{-1}\xi_x = \frac{\partial y}{\partial\eta}$, $J^{-1}\xi_y = -\frac{\partial x}{\partial\eta}$, $J^{-1}\eta_x = -\frac{\partial y}{\partial\xi}$, $J^{-1}\eta_y = \frac{\partial x}{\partial\xi}$.

3 HIGH ORDER DIFFERENCE METHOD

3.1 Summation by Parts (SBP) Property

For linear partial differential equations, well-posedness of the Cauchy problem or initial-boundary-value problems (IBVPs) can be proved by the energy method [11, 7]. The essential mathematical tool in the energy method for continuous problems is integration by parts

$$(u,v_x) \;=\; u(1)^Tv(1) - u(0)^Tv(0) \;-\; (u_x,v)\,. \tag{18}$$

Here u and v are differentiable d-dimensional real functions on $[0,1]$ and not to be confused with the u and v velocities of the 2D Euler equations. $(u,v)=\int_0^1 u^Tv\,dx$ is the L_2 scalar product and $||u||^2=(u,u)$ denotes the L_2 norm.

As an example, we consider the scalar linear advection equation

$$\begin{aligned} u_t + cu_x &= 0\,, & 0\le x\le 1\,, &\qquad (19)\\ u(x,0) &= f(x)\,, & 0\le x\le 1\,, &\qquad (20)\\ u(0,t) &= g(t)\,, & 0\le t\,, &\qquad (21) \end{aligned}$$

where the wave speed $c>0$ is constant. Applying the product rule, (19), (18) and (21), we obtain the equalities

$$\begin{aligned} \tfrac{d}{dt}||u(\cdot,t)||^2 \;&=\; 2(u,u_t) \;=\; -2c(u,u_x)\\ &=\; -c(u^2(1,t)-u^2(0,t)) \;=\; -cu^2(1,t)+cg^2(t)\,. \end{aligned} \tag{22}$$

Note that $u^T = u$ for the scalar problem (19). Integration over a time interval $[0, t]$ shows that the energy $\frac{1}{2}||u(\cdot, t)||^2$ can be estimated in terms of the initial condition (IC) and BCs. Thus, the problem is well-posed.

Assume the computational domain $[0, 1]$ is discretized by $N + 1$ grid points $x_j = jh$, $j = 0, 1, ..., N$, with $h = \frac{1}{N}$. Denote $v_j = v_j(t)$ as the approximations of $u(x_j, t)$ and $v = [v_0, v_1, ..., v_N]^T$. Kreiss and Scherer [12], Strand [23] and Carpenter et al. [1] constructed high order difference operators Q for "d/dx" such that the SBP property is satisfied, i.e.

$$(u, Qv)_h \;=\; u_N^T v_N - u_0^T v_0 \;-\; (Qu, v)_h \,, \tag{23}$$

where $u, v \in \mathbb{R}^{N+1}$. The discrete scalar product and norm are defined by

$$(u, v)_h \;=\; h u^T H v \,, \qquad ||u||_h^2 = (u, u)_h \,,$$

where H is a symmetric positive definite $(N + 1) \times (N + 1)$ matrix.

We employ a SBP operator Q, which is third-order accurate near the boundary and compatible with the standard sixth-order central difference operator in the interior. It was derived by Strand [23] and is of the form

$$(Q_x v)_j = \begin{cases} \frac{1}{h} \sum_{k=0}^{8} d_{jk} v_k, & j = 0, ..., 5, \\ (Q_x^{(6)} v)_j, & j = 6, ..., N-6, \\ -\frac{1}{h} \sum_{k=0}^{8} d_{N-j,k} v_{N-k}, & j = N-5, ..., N, \end{cases} \tag{24}$$

where $(Q_x^{(6)} v)_j = \frac{1}{h}(\frac{1}{60} v_{j+3} - \frac{3}{20} v_{j+2} + \frac{3}{4} v_{j+1} - \frac{3}{4} v_{j-1} + \frac{3}{20} v_{j-2} - \frac{1}{60} v_{j-3})$ is the standard sixth-order central difference approximation of the first derivative. The forms of the 5×9 matrix $D = (d_{jk})$ and matrix H can be found in [23][4][5]. Here H is a diagonal matrix defining the norm of the SBP operator Q. The global order of accuracy for (24) is four. Since (24) is based on a diagonal norm, its application to multi-dimensions is straightforward.

To closely maintain the order of accuracy of the scheme in curvilinear coordinates, the metric terms are discretized by the same difference operators as the flux derivatives in (25) below. In 3D, the Vinokur and Yee [26] treatment of the corresponding metric terms for freestream preservation is recommended.

In order to satisfy the discrete energy estimate, there are different ways of imposing the physical BCs in conjunction with the SBP operator Q to obtain strict linear stability [1][17][18]. The penalty method called "simultaneous approximation term" (SAT) of Carpenter et al. [1] or the projection method of Olsson [17][18] are two popular approaches. Either approach yields a discrete energy relation similar to the continuous energy relation. Nonlinear stability can be achieved by applying the boundary schemes to the in-going characteristic variables via the entropy splitting form of the inviscid flux derivatives. For simplicity, we have implemented the in-going Riemann invariants with the SAT method for the linearized Euler equations [16].

Thus, the spatial discretization of (17) yields the following semi-discrete equation for $\mathbf{U}'_{j,k}(t)$ approximating $\mathbf{U}'(j,k,t)$ with the index j,k suppressed

$$\mathbf{U}'_t = -\frac{J\beta}{\beta+1}(Q_\xi \hat{\mathbf{F}}'_1 + Q_\eta^{(6)} \hat{\mathbf{F}}'_2) - \frac{1}{\beta+1}(\nabla\xi \cdot \tilde{\mathbf{F}}_{\mathbf{W}} Q_\xi \mathbf{W} + \nabla\eta \cdot \tilde{\mathbf{F}}_{\mathbf{W}} Q_\eta^{(6)} \mathbf{W}) + SAT\,, \quad (25)$$

where

$$SAT = \begin{cases} -Jh_{00}^{-1}\mathbf{R}_0(\mathbf{\Lambda}_0^+ \mathbf{R}_0^{-1}\mathbf{U}'_0 - \mathbf{\Theta}_0(t))\,, & j=0, \\ 0\,, & 0<j<N, \\ Jh_{NN}^{-1}\mathbf{R}_N(\mathbf{\Lambda}_N^- \mathbf{R}_N^{-1}\mathbf{U}'_N - \mathbf{\Theta}_N(t))\,, & j=N, \end{cases}$$

with $J^{-1}\nabla\xi \cdot \mathbf{F}_\mathbf{U} = \mathbf{R}\mathbf{\Lambda}\mathbf{R}^{-1}$ the Jacobian matrix of the flux in the ξ-direction and $h_{00} = h_{NN}$ the first and last diagonal elements of norm matrix H. Note that the grid spacings $\Delta\xi$ and $\Delta\eta$ do not appear in (25), because they are chosen equal 1. The in-going characteristic variables $\mathbf{\Theta}_0(t)$ and $\mathbf{\Theta}_N(t)$ are prescribed as boundary conditions. Nonreflecting BC are simply implemented by $\mathbf{\Theta}_N(t) = 0$.

To get a discrete energy estimate, however, the SAT should rather be formulated in terms of the characteristic variables of $J^{-1}\nabla\xi \cdot \tilde{\mathbf{F}}_\mathbf{W}$, cf. (11). Since the eigenvalues and eigenvectors of that Jacobian matrix have not yet been expressed in closed form, they will be determined numerically by the cyclic Jacobi method such that the proper SAT can be used in the future.

3.2 Runge-Kutta Method

The ODEs (25) define the system of ODEs

$$\frac{d\mathbf{U}'}{dt} = \mathbf{R}(\mathbf{U}) + g(t)\,, \quad (26)$$

where $\mathbf{U}'$ is the vector of the difference approximations $\mathbf{U}'_{j,k}$ and $\mathbf{R}$ is the vector of the right hand sides of (25) except for the BC $g(t)$. Index j ranges from 0 to N, and because of the periodic boundary conditions in the circumferential η-direction index k goes from 3 to $K-3$. The ODE system (26) is solved by the classical fourth-order explicit Runge-Kutta method. The CFL condition for the numerical solution of (19) with periodic IC and BC is (e.g. [13]) $\sigma \leq 1.783$ for $Q_x^{(6)}$, where $\sigma = \frac{c\Delta t}{\Delta x}$ is the CFL number.

In order to maintain the global order of accuracy of the spatial difference operator and the Runge-Kutta temporal discretization, one needs to impose the time-dependent physical BC correctly (cf. [6], pp. 202-203). Incorrect implementation of a time-dependent Dirichlet BC lacks the 'errors' expected during the different stages of the Runge-Kutta method, because the inconsistency ruins the normal cancellation of errors to final global fourth-order spatial accuracy. Instead, the inconsistency leads to $\mathcal{O}(\Delta t)$ and thus $\mathcal{O}(\Delta x)$ at the boundary and $\mathcal{O}(\Delta x^2)$ globally independent of the high order finite difference

operator used. The problem and remedies are discussed in [2, 6, 9]. Here, we apply the treatment of $g(t)$ for a linear problem even to our nonlinear problem in each stage $(l), l = 0, 1, 2, 3$,

$$\begin{aligned} g^{(0)} &= g^n \,, \\ g^{(1)} &= g^n + \frac{\Delta t}{2} g'^n \,, \\ g^{(2)} &= g^n + \frac{\Delta t}{2} g'^n + \frac{\Delta t^2}{4} g''^n \,, \\ g^{(3)} &= g^n + \Delta t g'^n + \frac{\Delta t^2}{2} g''^n + \frac{\Delta t^3}{4} g'''^n \,, \end{aligned} \tag{27}$$

where $g^n = g(t_n)$. For a nonlinear problem, the accuracy will only be $O(\Delta t^2)$ at the boundary. A simple general treatment of $g(t)$ in the intermediate stages is not yet known for nonlinear problems [9]. Instead of computing the derivatives of $g(t)$ in (27) analytically, we use the fourth-order difference approximation [6]

$$\begin{pmatrix} g^{(0)} \\ g^{(1)} \\ g^{(2)} \\ g^{(3)} \end{pmatrix} = \begin{pmatrix} 0 & 1 & 0 & 0 \\ -\frac{1}{6} & \frac{3}{4} & \frac{1}{2} & -\frac{1}{12} \\ \frac{1}{12} & \frac{1}{4} & \frac{3}{4} & -\frac{1}{12} \\ -\frac{1}{12} & \frac{1}{4} & \frac{3}{4} & \frac{1}{12} \end{pmatrix} \begin{pmatrix} g(t_{n-1}) \\ g(t_n) \\ g(t_{n+1}) \\ g(t_{n+2}) \end{pmatrix} \tag{28}$$

3.3 Characteristic-Based Filter

For long time wave propagation of nonlinear systems, even with the absence of shock waves and/or steep gradients, spurious high frequency oscillations are generated by non-dissipative central spatial schemes. To suppress these spurious oscillations, a modified version of the Yee et al. [28] high order artificial compressibility method (ACM) filter scheme was used in [21]. For the present test problems, we employ a similar procedure, but the new filter has the form of the numerical dissipation proposed by Eriksson [3], however, not with a scalar but a matrix scaling similar to [15][21].

At the completion of a full step of the Runge-Kutta method, the numerical solution $\mathbf{U}'^{n+1}_{j,k}$ is filtered by a third-order difference operator

$$\tilde{\mathbf{U}}'^{n+1}_{j,k} \;=\; \mathbf{U}'^{n+1}_{j,k} \;-\; \Delta t \, J_{j,k} \, \left[D_\xi \mathbf{U}' \;+\; D_\eta \mathbf{U}' \right]^{n+1}_{j,k} \;. \tag{29}$$

$D_\xi \mathbf{U}'$ represents the fourth-order numerical dissipation in the ξ-direction defined by

$$D_\xi \mathbf{U}'_{\,j,k} \;=\; \kappa \, \delta_\xi^2 \, \mathbf{R}_\xi \, |\mathbf{\Lambda}_\xi| \mathbf{R}_\xi^{-1} \, \delta_\xi^2 \, \mathbf{U}'_{j,k} \tag{30}$$

with the difference operator $\delta_\xi \mathbf{U}'_{j,k} = \mathbf{U}'_{j+1/2,k} - \mathbf{U}'_{j-1/2,k}$. Eriksson chooses the boundary treatment of the numerical dissipation such that $-(U, D_\xi U)_h \leq 0$. Thus, we set

$\delta_\xi^2 \mathbf{U}'_{j,k} = 0$ for $j = 0$ and $j = N$, and replace $\kappa\,\delta_\xi^2 \mathbf{R}_{\xi j,k}...$ for $j = 0$ and $j = N$ by $\kappa\,(\mathbf{R}_{\xi 1,k}... - \mathbf{R}_{\xi 0,k}...)$ and $\kappa\,(\mathbf{R}_{\xi N-1,k}... - \mathbf{R}_{\xi N,k}...)$, respectively. The Jacobian matrix of the ξ-direction flux can be diagonalized as $\frac{\partial \hat{\mathbf{F}}_1}{\partial \mathbf{U}} = \mathbf{R}_\xi \mathbf{\Lambda}_\xi \mathbf{R}_\xi^{-1}$. The columns of $\mathbf{R}_\xi$ are the right eigenvectors of $\frac{\partial \hat{\mathbf{F}}_1}{\partial \mathbf{U}}$ and may be found in [26]. The eigenvalues of $\frac{\partial \hat{\mathbf{F}}_1}{\partial \mathbf{U}}$ define the diagonal matrix $\mathbf{\Lambda}_\xi = diag(u_\xi - c_\xi, u_\xi, u_\xi, u_\xi + c_\xi)$, where $u_\xi = uJ^{-1}\xi_x + vJ^{-1}\xi_y$, and $c_\xi = c\sqrt{(J^{-1}\xi_x)^2 + (J^{-1}\xi_y)^2}$. For our numerical experiments, the filter coefficient κ in the range of $0 < \kappa \leq\approx 0.02$ exhibits the desired property. For large gradients near the boundary, the present form of the filter proved to be more reliable than the form used in [15] [21], where no filter was applied at the boundaries.

For compatibility with the discrete energy estimate, we plan to formulate the filter in terms of the entropy vaiables $\mathbf{W}$ [4][5]

4 NUMERICAL RESULTS FOR KIRCHHOFF VORTEX SOUND

4.1 Analytical Solution

The Kirchhoff vortex is an elliptical patch (Fig. 1) with semi-major axis a and semi-minor axis b of constant vorticity $\boldsymbol{\nabla} \times \mathbf{u} = (0, 0, \omega)^T$ rotating with constant angular frequency $\Omega = \frac{ab}{(a+b)^2}\omega$ in irrotational flow [10]. We consider an almost circular Kirchhoff vortex of radius R, i.e. $a = R(1+\epsilon)$, $b = R(1-\epsilon)$, $0 < \epsilon \ll 1$.

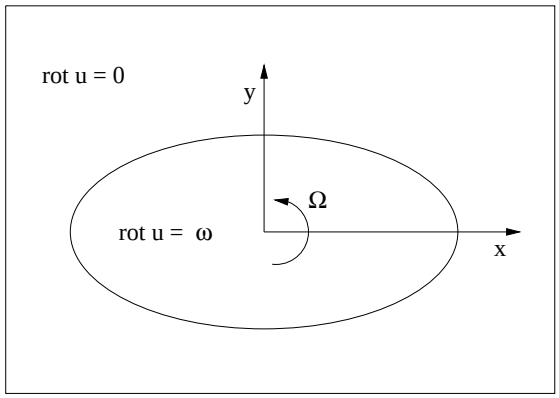

Figure 1: Kirchhoff vortex.

The 2D flow field constitutes an exact solution of the 2D incompressible Euler equations. The acoustic pressure generated by the Kirchhoff vortex is governed by the 2D Helmholtz equation, which can be solved analytically using separation of variables [14].

$$p'(r, \theta, t) \;=\; \Re(AH_2^{(1)}(kr)e^{i(2(\theta - \Omega t))}), \tag{31}$$

where

$$A = \frac{\rho_0 4R\epsilon\Omega^2}{kH_2^{(1)\prime}(kR)}$$

$\Re(z)$ denotes the real part of a complex number z. ρ_0 and c_0 are the stagnation density and speed of sound, respectively. $k = 2\Omega/c_0$ is the wave number. $H_2^{(1)}$ is the Hankel function of 2nd order.

The exact solution of the 2D linearized Euler equations for sound generated by the Kirchhoff vortex is determined by means of the exact solution of the Helmholtz equation (31) [15].

4.2 Kirchhoff Vortex Started Instantaneously

We consider the almost circular Kirchhoff vortex of example 2 in [14] with radius $R = 2m$, $\epsilon = 0.00125$, $\Omega = 2\,\pi\frac{1}{s}$. The stagnation conditions are $\rho_0 = 1.3\frac{kg}{m^3}$, $c_0 = 330\frac{m}{s}$. Thus, the Helmholtz number becomes $\mathcal{H} = kR = 2\Omega R/c_0 \approx 0.07616$. The difficulty with this test case is the large gradient of the acoustic pressure adjacent to the Kirchhoff vortex. Within the first $20\,m$, the modulus of the nondimensional acoustic pressure drops by two orders of magnitude. In the plots, the spatial coordinates are nondimensionalized by $R = 2m$, while the reference length $L = 1m$ is used in the computations. Density, velocity and pressure are nondimensionalized by ρ_0, c_0 and $\rho_0 c_0^2$, respectively. A polar grid stretched near the Kirchhoff vortex in the radial direction, and uniform in the circumferential direction of 129×42 is used, cf. Fig. 2 where only every fourth point in the radial direction every second point in the circumferential direction is shown.

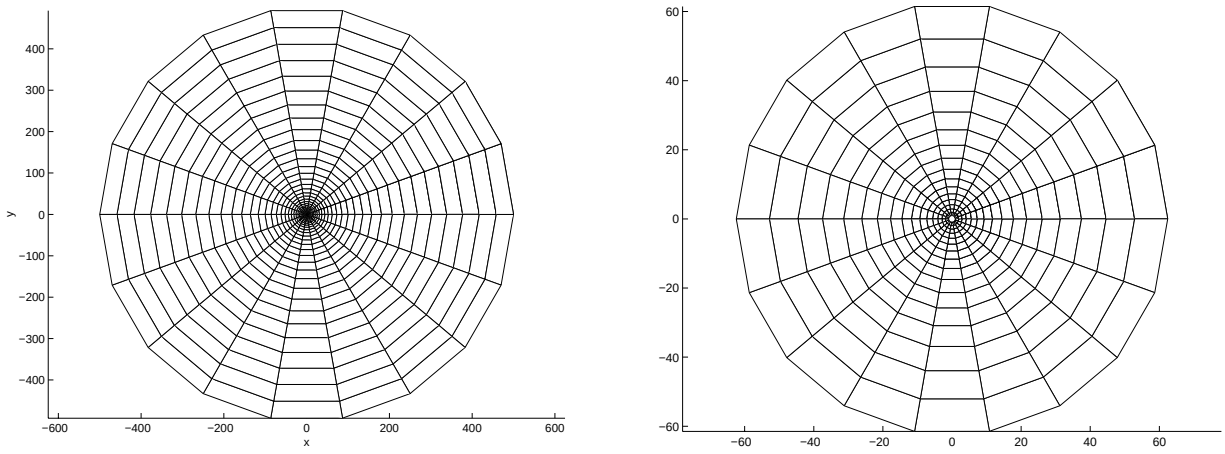

Figure 2: 129×42 grid and close-up.

We consider the Kirchhoff vortex starting instantaneously from stagnation conditions. The initial conditions are $\rho' = u' = v' = p' = 0$, except for the circle $r = R$, where the exact solution of the 2D linearized Euler equations for sound generated by the Kirchhoff vortex of Section 4.1 is prescribed at $t = 0$.

At first, we consider a mildly stretched grid in the radial direction between $r = 10$ and $r = 500$ to avoid the large gradients near $r = 1$. 65×24 grid points are used in the radial and circumferential directions. 500 time levels with time step $\Delta t = 3$ are computed. Without filter and without entropy splitting, the results are very poor. We compare the computed acoustic pressure at $t = 1500$ along the positive x-axis with the analytical solution in Fig. 3. The maximum error is 3 orders of magnitude larger than the maximum analytic acoustic pressure. The high frequency oscillations around the analytical solution decrease rapidly, and for $x \geq 75$, the computed acoustic pressure oscillates at least near the analytical solution. If the boundary conditions are not prescribed by the SAT method but injected after every final Runge-Kutta stage [15] [21], the maximum error is even 6 orders of magnitude larger than the maximum analytic acoustical pressure.

The wavefront started at $r = 10$ at $t = 0$ and propagating with the speed of sound in the radial direction would have reached $r = 760$ at $t = 1500$. In the plots at $r = 240$, we do not see an indication of a reflection of the wavefront at the farfield boundary $r = 500$.

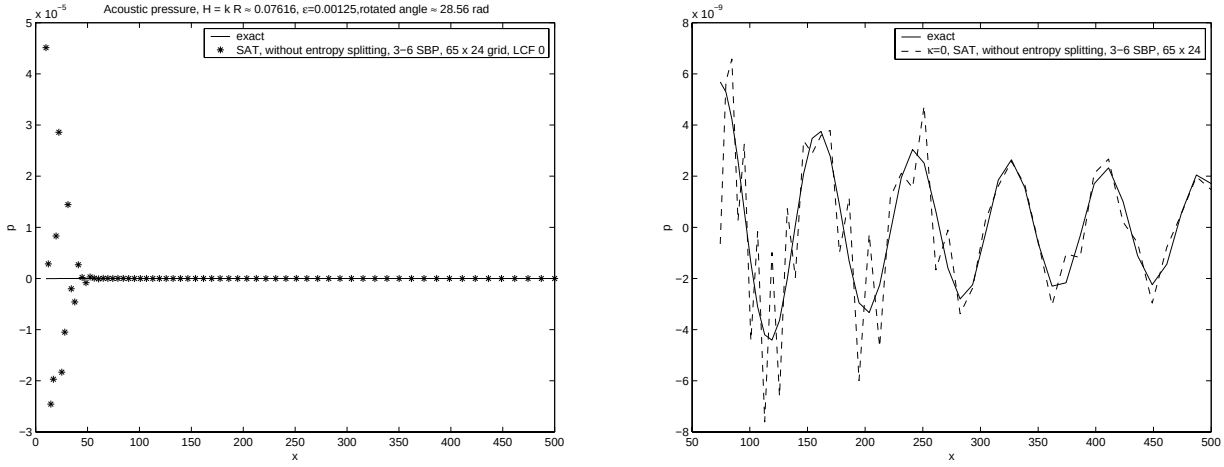

Figure 3: Acoustic pressure without filter and without entropy splitting for instantaneously started Kirchhoff vortex with $\mathcal{H} \approx 0.07616$, $\epsilon = 0.00125$, rotated angle $\approx 28.56 rad$.

With entropy splitting, the errors are much smaller, and the computed results are near the analytical solution everywhere in Fig. 4. For $x \geq 75$, the computed acoustic pressure oscillates slightly less than without entropy splitting. Entropy splitting with $\beta = 4$ was chosen, because Yee et al. [30] found that parameter to be optimal for vortex pairing in

a time-developing mixing layer. Thus, 80 % of the conservative flux derivative and 20 % of the non-conservative flux derivative are taken in (17).

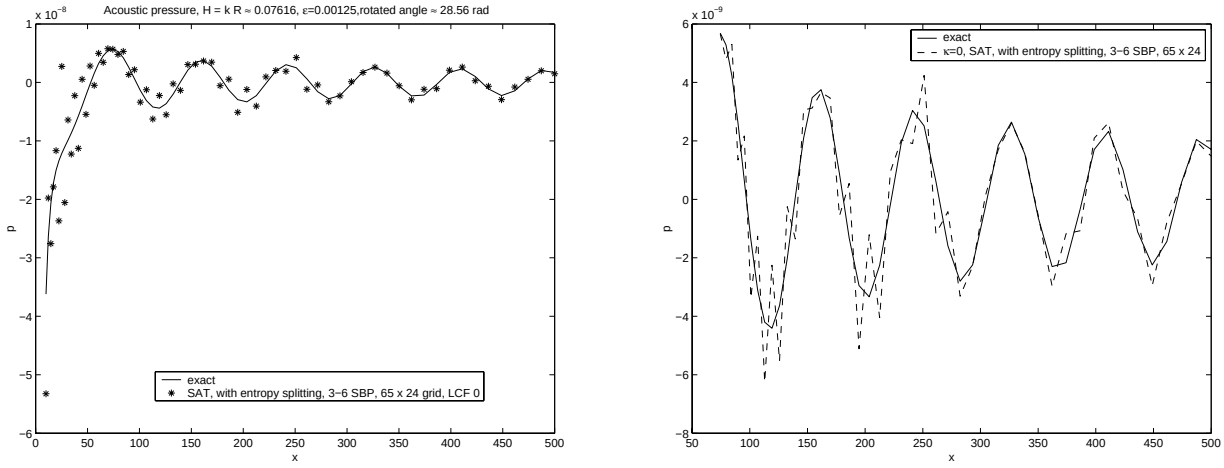

Figure 4: Acoustic pressure without filter and with entropy splitting $\beta = 4$ for instantaneously started Kirchhoff vortex with $\mathcal{H} \approx 0.07616$, $\epsilon = 0.00125$, rotated angle $\approx 28.56 rad$.

In [21], the filter (29) was used with

$$D_\xi \mathbf{U}'_{j,k} \;=\; \kappa\, \delta_\xi\, \mathbf{R}_\xi\, \mathbf{C}_\xi\, |\mathbf{\Lambda}_\xi| \delta_\xi^2\, \mathbf{R}_\xi^{-1} \delta_\xi\, \mathbf{U}'_{j,k} \tag{32}$$

where the lth diagonal element c^l of $\mathbf{C}_\xi$ is defined by $c^l_{j+1/2,k} = \max(\hat{\theta}_{j,k}, \hat{\theta}_{j+1,k})$ with $\hat{\theta}_{j,k} = \frac{|\,|\alpha^l_{j+1/2,k}| - |\alpha^l_{j-1/2,k}|\,|}{\max(|\alpha^l_{j+1/2,k}| + |\alpha^l_{j-1/2,k}|, 10^{-7})}$ and $\boldsymbol{\alpha}_{j+1/2,k} = \mathbf{R}_\xi^{-1} \delta_\xi \mathbf{U}'_{j+1/2,k}$. The metric terms in the filter where computed by the side normals of the centroid dual grid. For the filter in the ξ-direction, the term $\mathbf{R}_\xi\, \mathbf{C}_\xi\, |\mathbf{\Lambda}_\xi| \delta_\xi^2\, \mathbf{R}_\xi^{-1} \delta_\xi\, \mathbf{U}'_{j+1/2,k}$ was computed by considering the metric terms at $j + 1/2, k$ only. The filter in the ξ-direction was only applied at the interior grid points. The values of $\mathbf{U}'_{j,k}$ at $j = -1$ and $j = N + 1$ needed in (32) were obtained by zeroth-order extrapolation, e.g. $\mathbf{U}'_{-1,k} = \mathbf{U}'_{0,k}$. That filter worked well for simulating sound of a Kirchhoff vortex and an electric generator with $\mathcal{H} = kR = 2\Omega R/c_0 = 1$ [15][21]. However, for the present Kirchhoff vortex with the large gradients, that filter is not able to eliminate the high frequency oscillations even with a large filter coefficient $\kappa = 0.5$. Grid refinement helps a lot, but does not remove the oscillations near the boundary $x = 10$, cf. Fig. 5. p' along $\theta = 100°$ is compared in Fig. 6 as function of index $i = j + 1$. Little influence of the filter coefficient κ can be noticed for the coarse grid and a significant improvement with the finer grid.

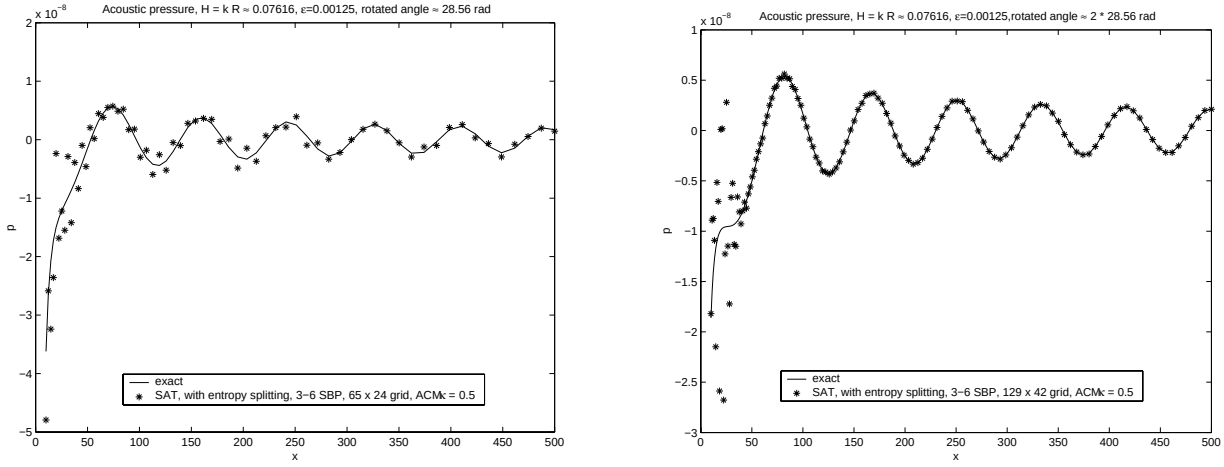

Figure 5: Acoustic pressure with filter (29) (32) and with entropy splitting $\beta = 4$ for instantaneously started Kirchhoff vortex with $\mathcal{H} \approx 0.07616$, $\epsilon = 0.00125$, rotated angle $\approx 28.56 rad$. 65×24 grid (left) and 129×42 grid (right).

Since the linear characteristic-based filter (29) with (30) is defined by the nodal values, it is computed with the metric terms computed with the high order difference method at the nodes. With $\kappa = 0.01$, quite accurate results are obtained even on the coarse 65×24 grid and excellent agreement with the analytical solution is found with the medium 129×42 grid, cf. Fig. 7. The errors are compared in Fig. 8.

In conjunction with the filter (29) with (30), the boundary implementation with injection proved to be slightly more accurate than SAT both without and with entropy splitting. The filter (29) with (32) gave good results using injection without entropy splitting. In that combination, filter (29) with (32) was slightly more accurate than (29) with (30) for the test case considered in [15][21].

Finally, using the filter (29) with (30) and the 129×42 grid in Fig. 2, it is possible to compute the Kirchhoff vortex sound from the source near $r = 1$ to the farfield $r = 500$. Fig.s 9 and 10 show the computed acoustic pressure along the positive x-axis and the computed acoustic pressure contours. Although there are still some oscillations present, the computed results match the analytical solution very well.

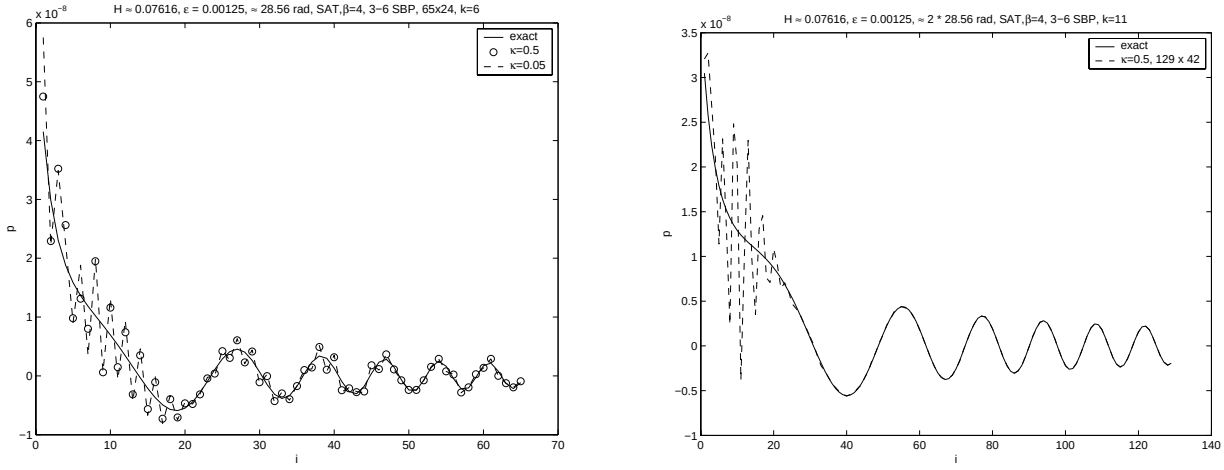

Figure 6: Acoustic pressure along $\theta = 100°$ with filter (29) (32) and with entropy splitting $\beta = 4$ for instantaneously started Kirchhoff vortex with $\mathcal{H} \approx 0.07616$, $\epsilon = 0.00125$, rotated angle $\approx 28.56 rad.$ 65×24 grid (left) and 129×42 grid (right).

5 CONCLUSIONS

The perturbation form of the entropy split 2D Euler equations has been formulated and tested for Kirchhoff vortex sound at low Mach numbers. The about 50% more CPU time needed for entropy splitting are paid off by much smaller spurious oscillations at large gradients. A new form of the filter operator has been devised which allows to compute low Mach number vortex sound with large gradients present.

In the future, higher order filter operators will be developed based on the entropy variables. The boundary conditions will be formulated in terms of the entropy variables as well to satisfy a discrete energy estimate. Thereby, we want to obtain a strictly stable high order difference method for low Mach number aeroacoustics even with the implementations of the boundary conditions and the filter included.

ACKNOWLEDGEMENTS

The collaboration with Dr. H.C. Yee, NASA Ames Research Center, is gratefully acknowledged. The research has been supported by TFR, the Swedish Research Council for Engineering Sciences, under the project 'Numerical Simulation of Vortex Sound'.

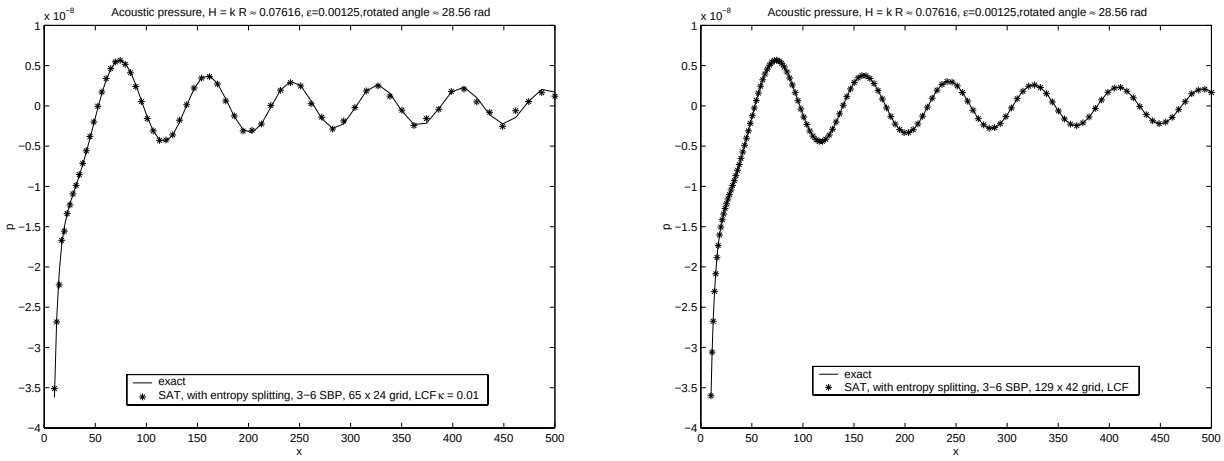

Figure 7: Acoustic pressure with filter (29) (30) and with entropy splitting $\beta = 4$ for instantaneously started Kirchhoff vortex with $\mathcal{H} \approx 0.07616$, $\epsilon = 0.00125$, rotated angle $\approx 28.56 rad$. 65×24 grid (left) and 129×42 grid (right).

REFERENCES

[1] Carpenter, M.H., Gottlieb, D., Abarbanel, S.: Time-Stable Boundary Conditions for Finite-Difference Schemes Solving Hyperbolic Systems: Methodology and Application to High-Order Compact Schemes. *J. Comput. Physics*, **111**, 220-236 (1994).

[2] Carpenter, M.H., Gottlieb, D., Abarbanel, S., Don, W.-S.: The Theoretical Accuracy of Runge-Kutta Time Discretization for the Initial Boundary Value Problem: A Study of the Boundary Error. *SIAM J. Sci. Comput.*, **16**, No. 6, 1241-1252 (1995).

[3] Eriksson, L.-E.: Boundary Conditions for Artificial Dissipation Operators. Technical Report FFA TN 1984-53, FFA, The Aeronautical Research Institute of Sweden, Stockholm, 1984.

[4] Gerritsen,M.: Designing an Efficient Solution Strategy for Fluid Flows. Ph.D. Thesis, Stanford University, Dec. 1996.

[5] Gerritsen,M., Olsson,P.: Designing an Efficient Solution Strategy for Fluid Flows. *J. Comput. Physics*, **129**, 245-262 (1996).

[6] Fornberg, B.: *A Practical Guide to Pseudospectral Methods*. First Paperback Edition, Cambridge University Press, Cambridge, 1998.

[7] Gustafsson, B., Kreiss, H.-O., Oliger, J.: *Time Dependent Problems and Difference Methods*. John Wiley & Sons, New York, 1995.

[8] Harten, A.: On the Symmetric Form of Systems for Conservation Laws with Entropy. *J. Comput. Phys.*, **49**, 151-164 (1983).

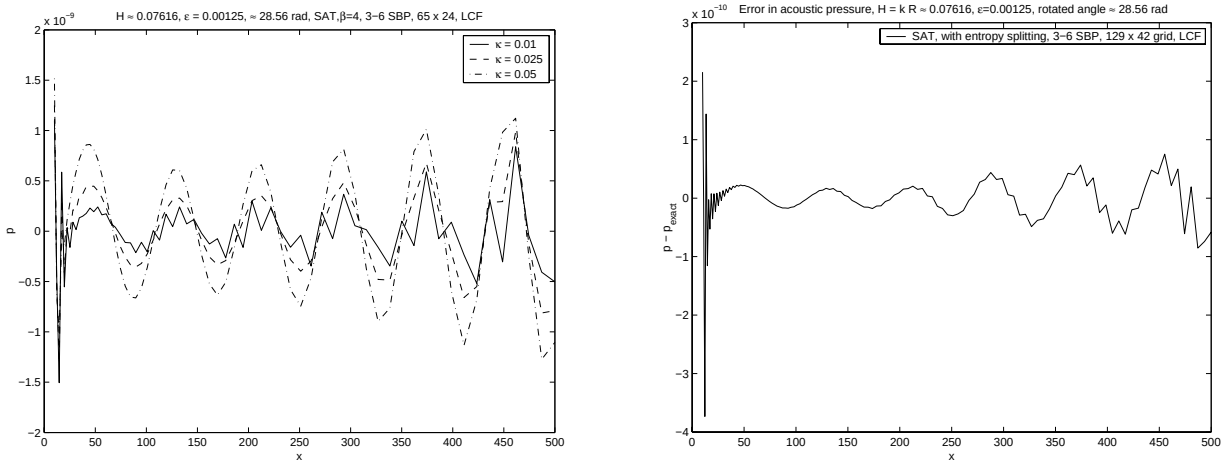

Figure 8: Error of acoustic pressure with filter (29) (30) and with entropy splitting $\beta = 4$ for instantaneously started Kirchhoff vortex with $\mathcal{H} \approx 0.07616$, $\epsilon = 0.00125$, rotated angle $\approx 28.56 rad$. 65×24 grid (left) and 129×42 grid (right).

[9] Johansson, M.: Loss of High Order Spatial Accuracy due to Boundary Error Caused by Runge-Kutta Time Integration. TechnicalReport 2000-013, Department of Information Technology, Uppsala University, May 2000. http://www.it.uu.se/research/reports/2000-013/

[10] Kirchhoff, G.: Vorlesungen über mathematische Physik. Mechanik. 2nd Edition, Leipzig 1877.

[11] Kreiss, H.-O., Lorenz, J.: *Initial-Boundary Value Problems and the Navier-Stokes Equations*. Academic Press, New York, 1989.

[12] Kreiss, H.-O., Scherer, G.: Finite Element and Finite Difference Methods for Hyperbolic Partial Differential Equations. In: Mathematical Aspects of Finite Elements in Partial Differential Equations, Academic Press, New York, 1974.

[13] Lele, S.K.: Compact Finite Difference Schemes with Spectral-like Resolution. *J. Comput. Physics*, **103**, 16-42 (1992).

[14] Müller, B.: On Sound Generation by the Kirchhoff Vortex. Report No. 209/ 1998, Department of Scientific Computing, Uppsala University, October 1998. http://www.tdb.uu.se/archive/reports/report-209-1998.ps.gz .

[15] Müller, B., Yee, H.C.: High Order Numerical Simulation of Sound Generated by the Kirchhoff Vortex. Technical Report 2001-004, Department of Information Technology, Uppsala University, Febr. 2001. http://www.it.uu.se/research/reports/2001-004/ . RIACS Technical Report 01.02, Jan. 2001. Submitted to Computing and Visualization in Science.

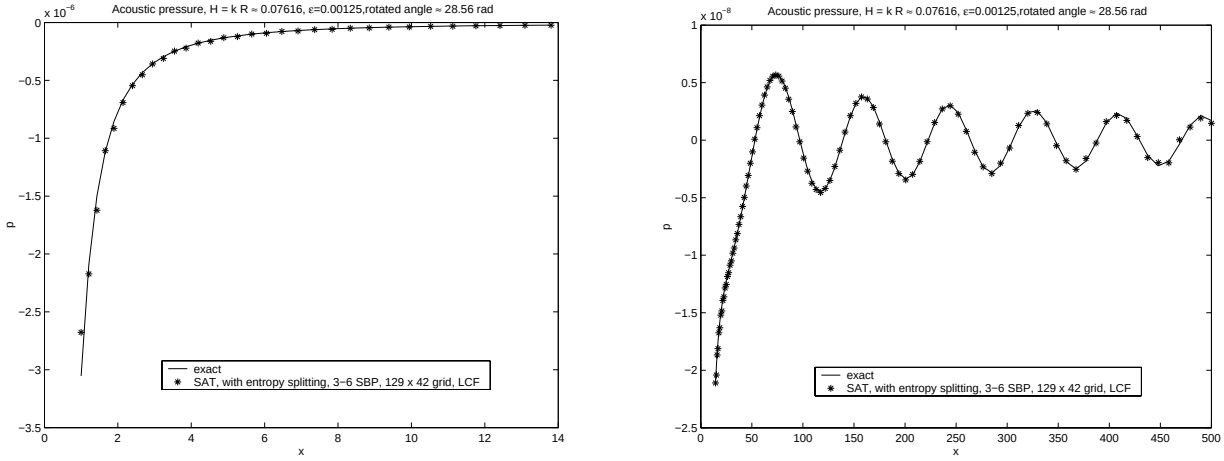

Figure 9: Acoustic pressure with filter (29) (30) and with entropy splitting $\beta = 4$ for instantaneously started Kirchhoff vortex with $\mathcal{H} \approx 0.07616$, $\epsilon = 0.00125$, rotated angle $\approx 28.56 rad$. 129×42 grid for whole problem.

[16] Nordström, J., Carpenter, M.H.: Boundary and Interface Conditions for High-Order Finite-Difference Methods Applied to the Euler and Navier-Stokes Equations. *J. Comput. Physics*, **148**, 621-645 (1999).

[17] Olsson,P.: Summation by Parts, Projections and Stability. I. *Math Comp.*, **64**, No. 211, 1035-1065 (1995).

[18] Olsson,P.: Summation by Parts, Projections and Stability. II. *Math Comp.*, **64**, No. 212, 1473-1493 (1995).

[19] Olsson,P.: Summation by Parts, Projections and Stability. III. RIACS Technical Report 95.06, 1995.

[20] Olsson,P., Oliger, J.: Energy and Maximum Norm Estimates for Nonlinear Conservation Laws. RIACS Technical Report 94.01, 1994.

[21] Polifke,W., Müller, B., Yee, H.C.: Sound Emission of Rotor Induced Deformations of Generator Casings AIAA Paper 2001-2274, 7th AIAA/CEAS Aeroacoustics Conference, May 28-30, 2001/Maastricht, The Netherlands. RIACS Technical Report 01.04, March 2001.

[22] Sesterhenn, J., Müller, B., Thomann, H.: On the Cancellation Problem in Calculating Compressible Low Mach Number Flows. *J. Comput. Physics*, **151**, 597-615 (1999).

[23] Strand, B.: Summation by Parts for Finite Difference Approximations for d/dx. *J. Comput. Physics*, **110**, 47-67 (1994).

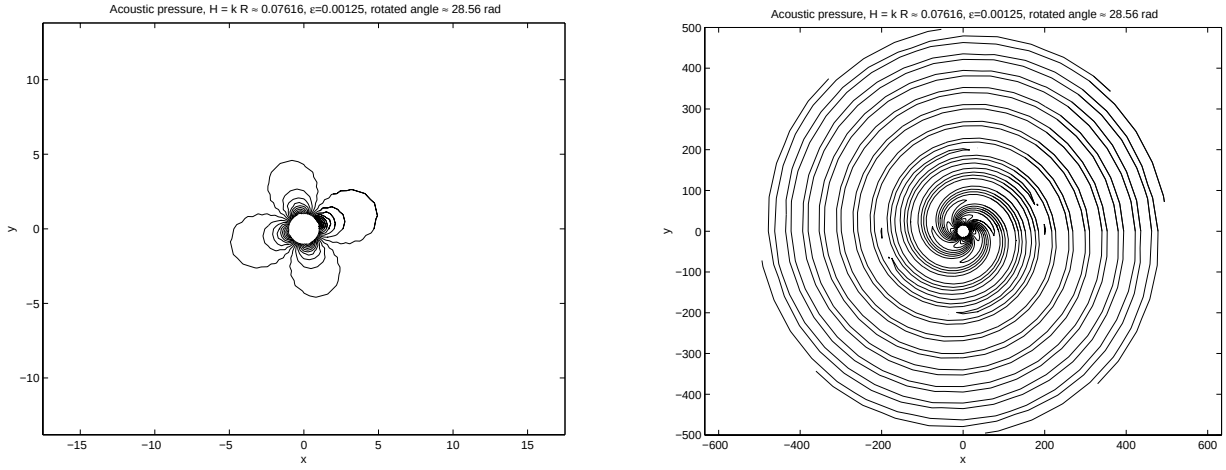

Figure 10: Acoustic pressure contours with filter (29) (30) and with entropy splitting $\beta = 4$ for instantaneously started Kirchhoff vortex with $\mathcal{H} \approx 0.07616$, $\epsilon = 0.00125$, rotated angle $\approx 28.56 rad$. 129×42 grid for whole problem.

[24] Strand, B.: Simulations of Acoustic Wave Phenomena Using High-Order Finite Difference Approximations. *SIAM J. Sci. Comput.*, **20**, 1585-1604 (1999).

[25] Tam, C.K.W.: Computational Aeroacoustics: Issues and Methods. *AIAA J.*, **33**, 1788-1796 (1995).

[26] Vinokur, M., Yee, H.C.: Extension of Efficient Low Dissipation High Order Schemes for 3-D Curvilinear Moving Grids. NASA TM 209598, 2000, and Proceedings of Computing the Future III: Frontiers in CFD - 2000, Half Moon Bay, CA, June 26-28, 2000.

[27] Wells, V.L., Renaut, R.A.: Computing Aerodynamically Generated Noise. *Annual Review of Fluid Mechanics*, **29**, 161-199 (1997).

[28] Yee, H.C., Sandham, N.D., Djomehri, M.J.: Low-Dissipative High-Order Shock-Capturing Methods Using Characteristic-Based Filters. *J. Comput. Physics*, **150**, 199-238 (1999).

[29] Yee, H.C., Sjögreen, B., Sandham, N.D., Hadjadj, A.: Progress in the Development of a Class of Efficient Low Dissipative High Order Shock-Capturing Methods. RIACS Technical Report 00.11, June, 2000 (http://www.riacs.edu/); Proceedings of the CFD for the 21st Century, July 15-17, 2000, Kyoto, Japan.

[30] Yee,H.C., Vinokur,M., Djomehri, M.J.: Entropy Splitting and Numerical Dissipation. *J. Comput. Physics*, **162**, 33-81 (2000).